LAWRENCE
LIVERMORE
NATIONAL
LABORATORY

LLNL-JRNL-644946

Ramp Compression of Diamond to 5 TPa: Experiments Taking Carbon to the Thomas-Fermi-Dirac Regime

R. F. Smith, J. H. Eggert, R. Jeanloz, T. S. Duffy, D. G. Braun, J. R. Patterson, R. E. Rudd, J. Biener, A. E. Lazicki, A. V. Hamza, J. Wang, T. Braun, L. X. Benedict, P. M. Celliers, G. W. Collins

October 16, 2013

Nature

Disclaimer

Ramp Compression of Diamond to 5 TPa: Experiments Taking Carbon to the Thomas-Fermi-Dirac Regime

R.F. Smith[1], J.H. Eggert[1], R. Jeanloz[3], T.S. Duffy[2], D.G. Braun[1], J.R. Patterson[1], R.E. Rudd[1], J. Biener[1], A.E. Lazicki[1], A.V. Hamza[1], J. Wang[2], T. Braun[1], L.X. Benedict[1], P.M. Celliers[1], G.W. Collins[1]

[1]Lawrence Livermore National Laboratory, P.O. Box 808, Livermore, CA 94550, USA
[2]Department of Geosciences, Princeton University, Princeton, NJ 08544, USA
[3]Department of Earth and Planetary Science, Department of Astronomy and Miller Institute for Basic Research in Science, University of California, Berkeley, CA 94720, USA

Thomas-Fermi-Dirac (TFD) theory, developed in the early days of quantum mechanics, is widely used to describe the bulk properties of matter at the high pressures existing deep inside large (e.g. extrasolar) planets and stars, where electrons are highly degenerate[1-9]. Recent developments in shock-free dynamic (ramp) compression provide the first laboratory access to this dense matter regime. We describe new ramp-compression measurements for diamond, achieving 3.7-fold compression at a peak pressure of 5 TPa (50 million atmospheres). These data, buttressed by first-principles density-functional calculations with the generalized gradient approximation, DFT-GGA[7], confirm that gradient-corrected TFD with correlation (TFD-Wc)[6] reproduces the equation of state and sound velocity of carbon at multi-TPa pressures. Our results provide experimental validation for the utility of this version of statistical-atom theory, and its application to planets, stars and inertial-confinement fusion[10]. Our data also furnish new constraints on mass-radius relationships for carbon-rich planets.

The recent discovery of hundreds of planets outside our Solar System[8,9] together with the significant push to achieve inertially confined fusion in the laboratory[10] has prompted a renewed interest in how matter behaves at millions to billions of atmospheres pressure. While the Thomas-Fermi-Dirac (TFD) statistical-atom model is widely used to describe the bulk properties of matter at these electron-degenerate conditions[1-9], theory and experiment suggest that new complexities may emerge at densities where core electrons – not just valence electrons – significantly influence the structure and bonding of matter[11].

Experimental access to multi-TeraPascal (TPa=10 million atmospheres) conditions common to the deep interiors of large planets is now possible with dynamic-ramped-compression. Dynamic compression is necessary to achieve atomic-scale pressures, conditions far beyond those accessible in static experiments[12,13]. Ramp compression produces less dissipative-heating, thus enabling higher compression and lower temperature, as compared to shock compression[14]. Ramp compression is however unstable relative to a shock because sound velocities typically increase with pressure,

so precise control of the applied pressure-loading history is required to achieve high pressures without shock formation.

The National Ignition Facility, a 2-MJ (megajoule) laser designed to create thermonuclear fusion in the laboratory[10], offers the energy and control necessary to ramp compress matter to several TPa. This report summarizes ramp-loading measurements on carbon to 5 TPa, with stress, density and sound speed data for the entire compression path. These new equation of state (EOS) data are at unprecedented conditions, and provide the first experimental constraints on fundamental quantum-statistical models for dense matter developed early in the last century.

In these experiments, 176 laser beams deliver a total of 2.2 TW peak power, with accuracy better than 1 percent in power and 0.02 ns in time, over 20 ns duration. The light hitting a target (indirectly) creates an ablatively driven pressure wave in the sample (Fig. 1), and – as pressure scales as the 7/8 power of the laser intensity[15] – the pressure is controlled to better than 1 percent. Samples consist of nanocrystalline diamond, shaped with steps so that the pressure-wave transit across four different thicknesses is recorded for each experiment[16]. Response of the sample is characterized by velocity interferometry (VISAR), which records the velocity of the sample's free (back) surface as it is engulfed by the pressure wave[17] (Fig. 1). Iterative Lagrangian analysis is used to translate these velocity data into a stress-compression (or stress-density) relation that quantifies the loading path (Fig. 2)[18,19]. These data are absolute — not referenced against a standard — which is important for quantifying the EOS and benchmarking condensed-matter theories in the TPa regime. We find a smooth variation of Lagrangian velocity with compression, and observe no evidence of phase transformation within the time-scale or resolution of our measurements (Fig. 2)[19].

In detail, we initiate loading with a ~ 0.1 TPa shock wave, before subjecting the sample to the main ramp compression (Fig. 1). Such pre-ramp loading of diamond produces a more fluid-like (strength-free) state[20] which is important for reducing the dissipative heating that can limit compression. Longitudinal stress (P_x) – not pressure – is shown in Fig. 2, as our one-dimensional loading method creates a uniaxial strain that relaxes toward an isotropic state.

A typical record (Fig. 1) shows a free-surface velocity profile, $u_{fs}(t)$, characterized by an initial shock to 4.1 km/s, followed by a fast rise and plateau at 7.2 km/s, and subsequent ramp compression to 46.6 km/s (3.7 TPa). Our analysis yields the Lagrangian sound speed C_L and P_x as functions of compression (ρ/ρ_0) or density (ρ) from the measured $u_{fs}(t)$ (Fig. 2)[18,19]. In all, three experiments yielded $C_L(\rho)$ and $P_x(\rho)$ to peak stresses of 2.7, 3.7 and 5 TPa, respectively. C_L decreases abruptly at u_{fs} = 4.1 km/s, corresponding to $P_{x,limit}$ = 0.11 TPa that is interpreted as the dynamic strength (elastic limit) of diamond[21]. Hydrodynamic simulations indicate that the rapid rise and plateau at 7.2 km/s corresponds to a reverberating compression wave within the intermediate Au layer.

These new data are used to test several carbon EOS models into the multi-TPa regime (Fig. 2)[19]. First, an isentrope derived from first-principles density functional theory (DFT-GGA) is in good agreement with an isentrope estimated from a Mie–

Grüneisen reduction and extrapolation of shock-Hugoniot data collected to 2 TPa. For reference, the corresponding Hugoniots are shown (solid red and yellow curves), and illustrate the uncertainties in extrapolating the shock-compression EOS of carbon. Not shown are extrapolations of static-compression and elasticity measurements to 0.14 TPa, the most recent version of which (Vinet EOS with preferred values of zero-pressure bulk modulus and pressure derivative of K_0 = 445 GPa and K'_0 = 4.2)[22] is indistinguishable from the isentropes presented here (the difference between isentropes and isotherms is also indistinguishable on this scale). However, such extrapolations are highly uncertain: depending on the EOS used (e.g., Vinet with K_0 = 445 GPa and K'_0 = 3.0 or with K_0 = 445 GPa and K'_0 = 4.2)[22,23], the isentrope pressure at a density of 12 g/cm^3 can range between 2.8 and 5.7 TPa (Fig. 3, inset). In short, our new data are compatible with published experimental and theoretical results, but lie in a regime requiring significant extrapolation from prior measurements.

Also consistent with estimated isentropes is the gradient- and correlation-corrected Thomas-Fermi-Dirac equation of state (TFD-Wc) between about 2 and 5 TPa (Fig. 2 and Fig. S3[19]). The agreement with DFT is notable, because the statistical-atom model considers neither crystal structure nor orbital information whereas DFT includes both. We acknowledge that the agreement may be partly fortuitous because carbon might not yet be in its densest crystal structure at these pressures, and the deviation of statistical-atom theories is toward predicting compressions that are systematically too low (see upper inset of Fig. 2b). For the different TF models we use the reference density of diamond to plot these models in compression (Fig. S3 shows similar plot in stress density).[19]

Our ramp-compression data achieve higher densities than shock compression, consistent with temperatures being lower than on the Hugoniot.[14,19] Moreover, these new data are comparable to cold-isothermal compression calculations with DFT-GGA over most of the pressure range studied, TFD-W and TFD-Wc at pressures above ~2 TPa, but not with Thomas-Fermi or other TFD results.[19] Because both strength and heating can stiffen the stress–compression relation with respect to the isentrope[24] our data should be considered an upper bound for such comparison, and further study is warranted to better characterize this convergence of theory and experiment.

The experimental techniques developed here provide a new capability to experimentally access pressures deep in planetary interiors. Carbon is the fourth most abundant element in the cosmos and plays a potentially important role in many types of planets, both within and outside the Solar System. One proposed group of super-Earth exoplanets (1-10 Earth masses in size) are those enriched in carbon, and the planet 55 Cancri e has been proposed as a possible carbon planet[29]. Figure 3 shows mass-radius relationships for selected known super-Earths together with various hypothetical uniform-composition planets, including a pure carbon planet based on our ramp compression equation of state. Using the new data we find the central pressure for a 10 Earth-mass pure carbon planet to be ~900 GPa. This new capability to reach multi-TPa pressures enables experimental access to Jupiter's core pressures where extrapolations of earlier shock (yellow band) and static (grey band) data become unreliable (Fig. 3, inset)[30].

Our results also have relevance for large pulsar planets, such as the companion of millisecond pulsar PSR J1719-1438[25]. This object has a minimum mass somewhat larger than Jupiter ($1.15*10^{-3}$ M_{Sun} or 383 Earth masses), and a 2.2 hour orbital period. A carbon-rich composition was suggested based on TFD-Wc results for carbon (Refs. 6 and 28). The reliability of this form of TFD theory as shown by our experiments supports this interpretation. An extrapolation of our EOS consistent with TFD-Wc suggests an object of this mass made of pure carbon would have a radius of ~4.3 Earth radii and a central pressure of ~200 TPa. The mean density of 27 g/cm^3 is consistent with the measured minimum density of the pulsar planet (23 g/cm^3)[28].

In summary, diamond, the least compressible material known, was compressed to an unprecedented density of 12 g/cm^3, more than that of lead at ambient conditions. The measured Lagrangian sound speed, stress and compression provide the first experimental data for constraining condensed-matter theory and planet-evolution models in the TPa regime. By realizing three necessary conditions, 1) the adiabatic conditions of dynamic compression; 2) a loading profile soft enough to avoid shock formation; and 3) a nearly fluid-like response of the sample, such that strength and dissipation are minimal, these experiments document an approach for taking solids to the long-sought high-density conditions of statistical-electron theory.

1. Thomas, L. H. The calculation of atomic fields. *Math. Proc. Cambridge Phil. Soc.* **23**, 542-548 (1927).
2. Dirac, P. A. M. Note on exchange phenomena in the Thomas atom. *Math. Proc. Cambridge Phil. Soc*. **26**, 376-385 (1930).
3. Feynman, R. P., Metropolis N. & Teller, E. Equation of state of elements based on the generalized Fermi-Thomas theory. *Phys. Rev.* **75**, 1561-1573 (1949).
4. Salpeter E. E. & Zapolsky, H. S. Theoretical high pressure equations of state, including correlation energy. *Phys. Rev.* **158**, 876-886 (1967).
5. Abrahams A. M. & Shapiro, S. L. Cold equation of state from Thomas-Fermi-Dirac-Weizsacker theory. *Phys. Rev. A* **42**, 2530-2538 (1990).
6. Lai, D., Abrahams, A. M. & Shapiro, S. L. Equation of state in metals and cold stars: Evaluation of statistical models. *Astrophys. J.* **377**, 612-628 (1991).
7. Correa, A. A., Benedict, L. X., Young, D. A., Schwegler, E. & Bonev, S. A. A first principles multi-phase equation of state of carbon under extreme conditions. *Phys. Rev B* **78**, 024101 (2008).
8. Swift, D. C. *et al.* Mass-radius relationships for exoplanets. *Astrophys. J.* **744**, 59-68 (2012).
9. Seager, S. Exoplanet habitability. *Science* **340**, 577 (2013).
10. Edwards, M. J. *et al.* Progress towards ignition on the National Ignition Facility. *Phys. Plasmas* **20**, 70501 (2013).
11. Pickard C.J. & Needs R.J. Aluminium at terapascal pressures. *Nature Materials* **9**, 624 (2010).
12. The quantum-mechanical "pressure" $h^2/(16\pi^3 m_e a_0^5)$ = 2.34 TPa counteracts the electron's Coulomb attraction to the nucleus for the Bohr model of the atom at

ambient conditions: h, m_e and a_0 are Planck's constant, the mass of the electron and the Bohr radius (i.e., the quantum of action, and atomic units of mass and length, respectively). At these pressures, the properties of atoms themselves change.

13. Dubrovinsky, L., Dubrovinskaia, N., Prakapenka, V. B. & Abakumov, A. M. Implementation of micro-ball nanodiamond anvils for high-pressure studies above 6 Mbar. *Nature Comm.* **3**, 1163 (2012).
14. Zel'dovich, Ya. B. & Raizer, Yu. P. *Physics of Shock Waves and High-Temperature Hydrodynamic Phenomena*, Dover (2002).
15. Atzeni S. & Meyer-ter-Vehn, J. *The Physics of Inertial Fusion*, Oxford University Press, (2004).
16. Our samples consist of a 50-μm thick diamond plate used as an ablator, a 10-μm Au layer pre-heat shield, and a diamond plate having four steps (Fig. 1 inset). The diamond was synthesized by chemical vapor deposition to yield a layered microstructure with an average grain size of 200 nm and a density of 3.25 g/cm^3 (± 0.01%) [Reichart, P. *et al.* Three-dimensional hydrogen microscopy in diamond. *Science* **306**, 1537 (2004); Dawedeit, C. *et al*. Grain size dependent physical and chemical properties of thick CVD diamond films for high energy density physics experiments, *Diamond and Related Materials*, accepted]. The final sample had alternating 0.35 μm layers of 20 nm grains and ~350 nm grains. X-ray diffraction showed a <110> texture in the growth direction. The thickness of the sample is determined to ± 1.0 μm, including uncertainties in the diamond ablator and Au thicknesses, whereas the differences in step thickness are determined by optical interferometry to ± 0.1 μm.
17. The VISAR (Velocity Interferometer System for Any Reflector) diagnostic uses a line-focused 660 nm-wavelength laser beam to monitor a ~1 mm strip across all four steps of the sample [Celliers P. M. *et al*. Line-imaging velocimeter for shock diagnostics at the Omega laser facility. *Rev. Sci. Instrum.* **75**, 4916 (2004)]. Changes in velocity of the diamond free surface produce phase shifts in interference fringes that are recorded with a streak camera (Fig. 1). A typical VISAR record has a 5 μm spatial resolution, a 10 ns streak window with 0.01 ns resolution, and a velocity resolution of 0.1 km/s.
18. Rothman, S. D. *et al.* Measurement of the principle isentropes of lead and lead-antimony alloy to ~400 kbar by quasi-isentropic compression. *J. Phys. D*, **38**, 733-740 (2005).
19. See Supplementary Material.
20. McWilliams, R. S. *et al.*, Strength effects in diamond under shock compression from 0.1 to 1 TPa. *Phys. Rev. B* **81**, 014111 (2010).
21. The corresponding dynamic yield strength (Y_0) is determined from $Y_0 = P_{x,limit}\ (1 - 2\nu)/(1 - \nu)$, with the Poisson ratio $\nu = 0.18$ derived from our sound-speed data (Fig. 2(a)) from $(C_{longitudinal}/C_{bulk})^2 = 3\ (1 - \nu)/(1 + \nu)$. This yields $Y_0 = 0.085$ TPa, which is less than observed in static experiments ($Y_0 = 0.13$–0.14 TPa [Eremets, M. I. *et al.* The strength of diamond. *Appl. Phys. Lett.* **87**, 141902 (2005)]) but consistent with

the values $0.069 < Y_0$ (TPa) < 0.096 reported for ramp compression of diamond with micron grain size[20].
22. Dewaele, A., Datchi, F., Loubeyre, P. & Mezouar, M. High pressure-high temperature equation of state of neon and diamond. *Phys. Rev. B* **77**, 094106 (2008).
23. Occelli, F., Loubeyre, P. & Letoullec, R. Properties of diamond under hydrostatic pressures up to 140 GPa. *Nature Mater.* **2**, 151 (2003).
24. Hicks, D. G. *et al.* High-precision measurements of the diamond Hugoniot in and above the melt region. *Phys. Rev.* B **78**, 174102 (2008).
25. Wolszczan, A. & Frail, D. A planetary system around the millisecond pulsar PSR1257 + 12. *Nature* **355**, 145 (1992).
26. Martinez-Canales, M., Pickard, C. J. & Needs, R. J. Theormodynamically stable phase of carbon at multiterapascal pressures. *Phys. Rev. Lett.* **108**, 045704 (2012).
27. F. W. Wagner, F. Sohl, H. Hussmann, M. Grott, and H. Rauer, Interior structure models of solid exoplanets using material laws in the infinite pressure limit. Icarus, 214, 366-376 (2011).
28. Bailes, M. *et al.* Transformation of a star into a planet in the millisecond Pulsar binary. *Science* **333**, 1717-1720 (2011).
29. Madhusudhan, N., Lee, K. K. M. & Mousis O. A possible carbon-rich interior in super-earth 55 Cancri e, Astrophys. J. Lett. **759**, L40 (2012).
30. Nettelmann, N. *et al.* Ab initio equation of state data for hydrogen, helium, and water and the internal structure of Jupiter. Astrophys. J. **683**, 1217–1228, (2008).

Acknowledgments: We thank Christoph Wild (Fraunhofer Institute for Applied Solid-State Physics, Freiburg, Germany) for preparation of the diamond targets. This work was performed under the auspices of the U.S. Department of Energy by Lawrence Livermore National Laboratory under Contract No. DE-AC52-07NA27344, with additional support from the Department of Energy, the University of California, and the Miller Institute for Basic Research in Science.

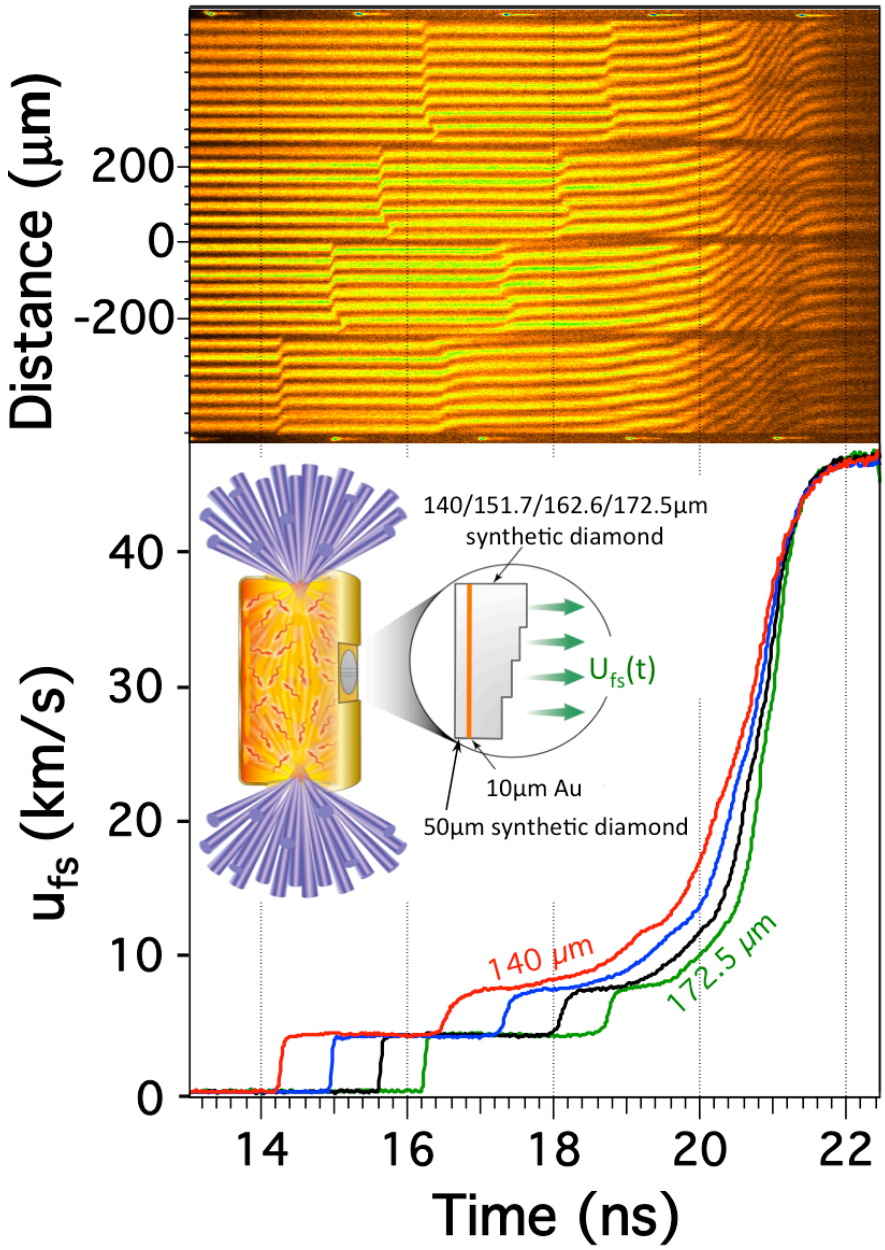

Fig. 1. Velocity interferometry record (*top*) and derived free-surface velocity u_{fs} (*bottom*) as a function of time for diamond compressed at NIF. The target (*inset*) consists of a 6-mm diameter by 11-mm long Au cylinder (hohlraum), inside of which the 351-nm wavelength laser light (*purple beams*) is converted to x-ray energy that is absorbed by the diamond sample placed on the side of the hohlraum. The x-rays ablate and ramp-compress the sample, and the free surface velocity is recorded for four thicknesses of diamond: 140.0 μm (*red*), 151.7 μm (*blue*), 162.6 μm (*black*) and 172.5 μm (*green*).

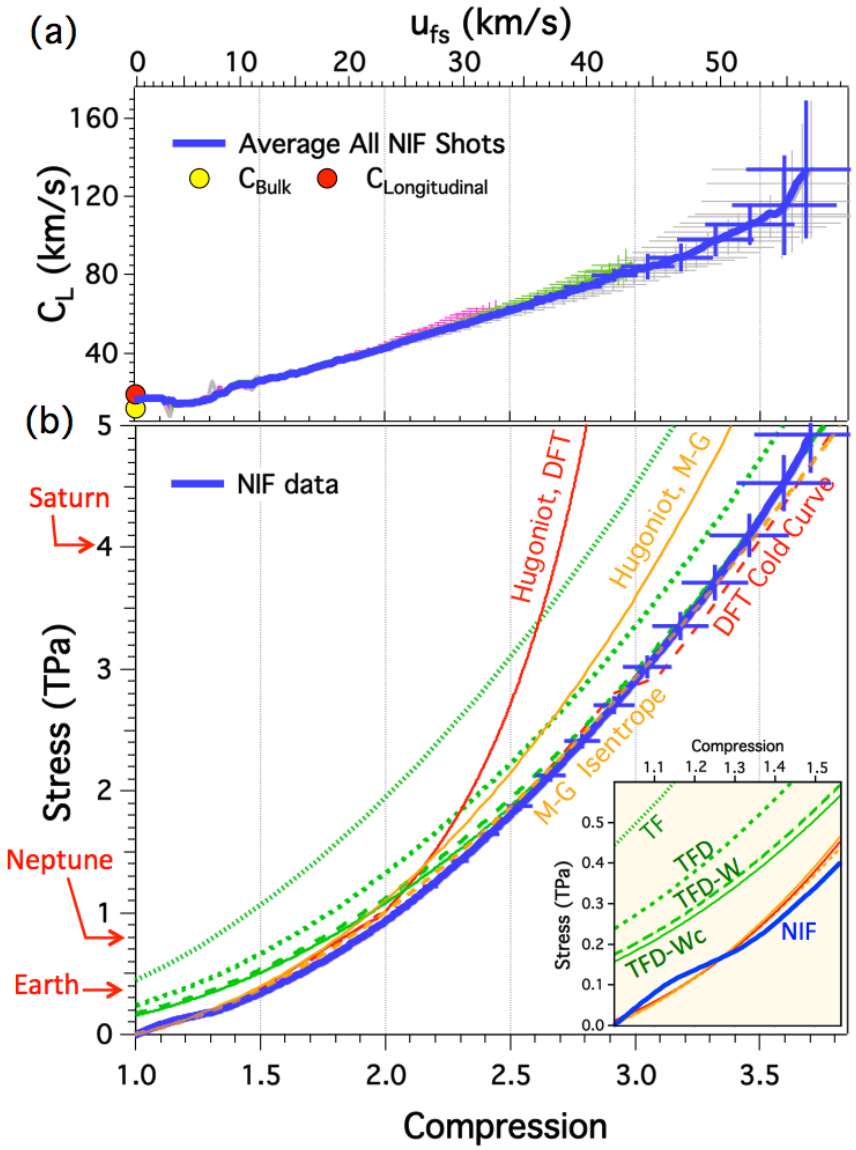

Fig. 2. Lagrangian sound velocity C_L, (*a*) and longitudinal stress P_X (*b*) as functions of compression determined from the velocity interferometry records (Fig. 1). Three experiments (N110308, N110516, N110524) yield Lagrangian-velocity data (*pink, light-green, grey* in (*a*)), and their average (*dark blue curve* in (*a*) and (*b*)), including projected uncertainties, are used to determine the stress-compression path (For stress density comparison see text and Supplementary Material)[18,19]. Model comparisons include: i) estimates of the shock-compression Hugoniots from density functional theory (DFT, *solid red curve*), and extrapolated from experimental data below 2 TPa (*yellow solid curve*); ii) the isentrope from DFT (*red dashed curve*), and derived from the extrapolated experimental Hugoniot (*yellow dashed curve*) using a simple Mie-Gruneisen model; iii) 0 K isotherms obtained from the statistical-atom models (TF, TFD, TFD-W, and TFD-Wc) as *green dotted, short dashed, long dashed, solid, and dot-dashed curves*)[6]. To present these Thomas-Fermi based isotherms in compression we use the initial density of diamond as the reference density[19]. Central pressures for Earth, Neptune and Saturn are shown for reference[8]. Inset in (*b*) shows detailed comparisons between measurements and models at low pressure.

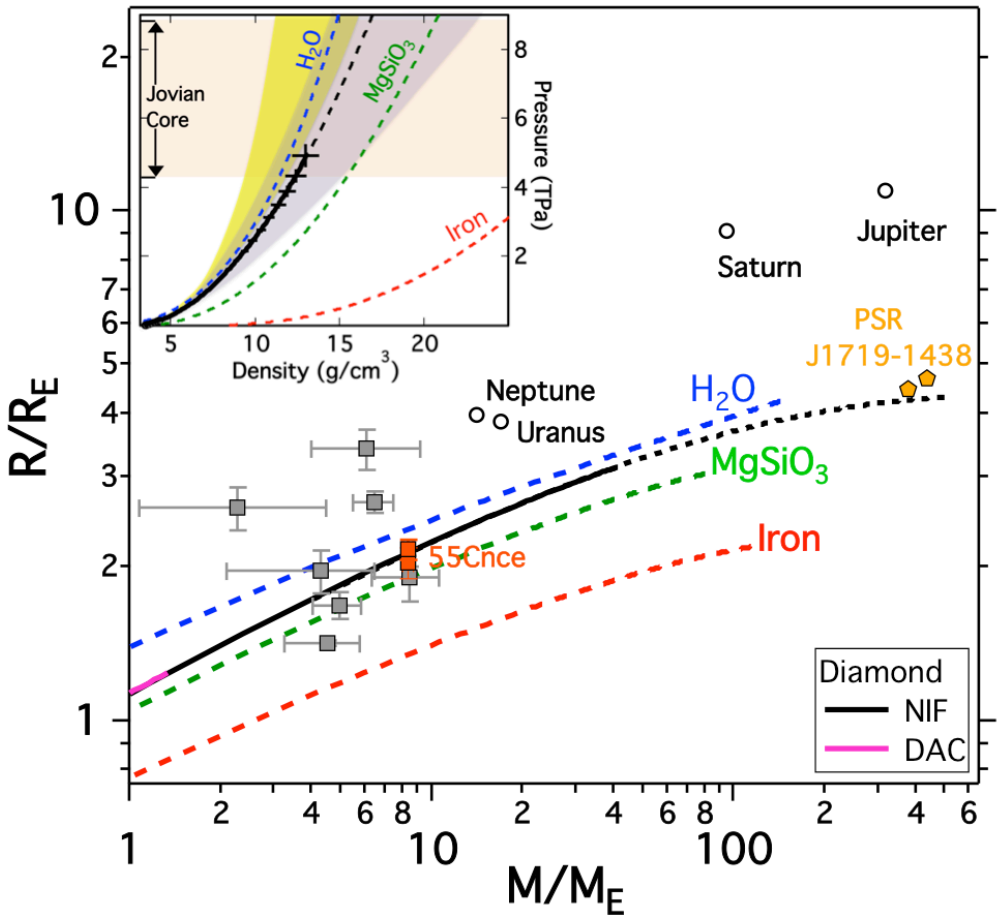

Fig. 3. Mass-radius relationships for homogenous-composition planets, including for pure carbon (*black curve*) based on the present experimental data (this study), as well as for H_2O (*blue curve*), post-perovskite $MgSiO_3$ (*green curve*) and iron (*red curve*)[27] (curves are dashed when based on extrapolated EOS data). Yellow symbols show mass and radii values consistent with the minimum density for the companion object to pulsar PSR J1719-1438 for assumed oribtal inclinations of 90 and 60 degrees.[28] The grey squares with error bars show masses and radii of selected transiting super Earths. Two possible values of radii are shown for 55 Cancri e (*red squares*)[29] . The inset shows the pressure-density equation of state at conditions relevant to Jupiter's core (~4.3-8.8 TPa)[30]. Black curve with error bar shows the density scaled ramp compression diamond data from this study up to 5 TPa, thereby achieving pressures of Jupiter's core. Also shown are a range of different extrapolations of shock data (yellow band, see suppl. material) and DAC data at 300 K (grey band).[22,23] Dashed curves are extrapolations of the EOS for representative materials used for constructing the Jovian core[30].

Supplementary Materials for:

Ramp Compression of Diamond to 5 TPa: Experiments Taking Carbon to the Thomas-Fermi-Dirac Regime

R.F. Smith[1], J.H. Eggert[1], D.G. Braun[1], J.R. Patterson[1], R.E. Rudd[1], R. Jeanloz[3], T.S. Duffy[2], J. Biener[1], A.E. Lazicki[1], A.V. Hamza[1], J. Wang[2], T. Braun[1], L.X. Benedict[1], P.M. Celliers[1], G.W. Collins[1]

[1]Lawrence Livermore National Laboratory, P.O. Box 808, Livermore, CA 94550, USA
[2]Department of Geosciences, Princeton University, Princeton, NJ 08544, USA
[3]Department of Earth and Planetary Science, Department of Astronomy and Miller Institute for Basic Research in Science, University of California, Berkeley, CA 94720, USA

1. Determination of Stress-Density Relation

The Lagrangian analysis method developed by Aidun and Gupta[1] and modified by Rothman[2] was used to determine the Lagrangian sound speed $C_L(u)$ and the stress-compression (P_x-ρ/ρ_0) from the measured $u_{fs}(t)$ data, where u is the particle speed, and u_{fs} is the samples free surface velocity (with 4 steps, in the present experiments). Metrology of the sample surface showed that the roughness was < 0.1 μm, thickness gradients were < 1%, and step heights were accurate to within 0.1 μm. In all, three shots gave $C_L(u)$ and P_x-ρ/ρ_0 data. $C_L(u)$ and its uncertainty $\sigma_{C_L}(u)$ are obtained from thickness and velocity vs time data by linear regression using errors determined by our measurement accuracies: u_{fs} (0.05 km/s), time (10 ps), and step height (100 nm). The uncertainty is propagated by calculating the weighted mean average of all three shots, $\langle C_L(u)\rangle = \sum_j \frac{C_{L,j}}{\sigma^2_{C_{L,j}}} / \sum_j \frac{1}{\sigma^2_{C_{L,j}}}\Big|_u$ as shown by the blue curve in Fig. 2(a), where j is the shot number. The uncertainty in the average value is chosen from the maximum of the uncertainty in the mean and the weighted standard deviation. $\langle C_L(u)\rangle$ and $\sigma_{\langle C_L\rangle}$ are integrated to obtain $P_x = \rho_0 \int_0^u \langle C_L\rangle \, du$, $\rho = \rho_0 \left(1 - \int_0^u \frac{du}{\langle C_L\rangle}\right)^{-1}$, and their uncertainties $\sigma_{P_x} = \rho_0 \int_0^u \sigma_{\langle C_L\rangle} du$ and $\sigma_\rho = \frac{\rho^2}{\rho_0} \int_0^u \frac{\sigma_{\langle C_L\rangle} du}{\langle C_L\rangle^2}$. Uncertainties are propagated though the integrals

linearly, rather than in quadrature because $\sigma_{\langle C_L \rangle}$ appears to be strongly correlated rather than random. This method of uncertainty propagation allows the direct propagation of experimental uncertainties to $P_x - \frac{\rho}{\rho 0}$ *or* $P_x \quad - \rho$.

Release waves from the diamond-vacuum interface significantly perturb the incoming ramp wave. Extensive tests using simulated data confirm that the iterative Lagrangian analysis accurately corrects for these wave interactions.

2. Mie-Grüneisen Hugoniot and isentrope.

In the main text (Fig. 2) we compare our stress-compression data to a Mie-Grüneisen Hugoniot and isentrope reduced from available diamond Hugoniot data. There are several ways to construct a Mie-Grüneisen equation of state, and here we begin with the relation for the pressure relative to a reference pressure P_{ref},

$$P(\eta, E) = P_{\text{ref}}(\eta) + \rho_0 \eta \gamma \left(E - E_{\text{ref}}(\eta)\right), \tag{1}$$

where, $\eta = \frac{\rho}{\rho_0}$ is the compression, γ is the Grüneisen parameter which is assumed to depend only on density, and ρ_0 is the initial density. We can use either the Hugoniot or isotherm data to determine the reference states. Here we use the diamond Hugoniot data as the reference using a linear fit to existing shock velocity versus particle velocity data[3-8],

$$Us = C + sUp \tag{2}$$

where, C=12.0, and s=1.04. From this we obtain,

$$P_{ref}(\eta) = \rho_0 \eta \frac{C^2(\eta - 1)}{\left(\eta - s(\eta - 1)\right)^2}, \tag{3}$$

$$E_{ref}(\eta) = \rho_0 \eta \gamma \left[E - \frac{C^2(\eta - 1)^2}{2\left(\eta - s(\eta - 1)\right)^2} \right]. \tag{4}$$

Finally from Eq. 1 we obtain the cold curve

$$P_0(\eta) = \rho_0 \eta \left(\frac{C^2(\eta - 1)}{\left(\eta - s(\eta - 1)\right)^2} + \gamma \left(E_0 - \frac{C^2(\eta - 1)^2}{2\left(\eta - s(\eta - 1)\right)^2} \right) \right), \tag{5}$$

where we solve

$$\frac{dE_0}{d\eta} = \frac{1}{\rho_0 \eta^2} \left(P_H(\rho) + \rho_0 \gamma \eta \left(E_0 - E_H \right) \right) = \frac{1}{\eta} \left(\frac{C^2(\eta - 1)}{\left(\eta - s(\eta - 1)\right)^2} + \gamma \left(E_0 - \frac{C^2(\eta - 1)^2}{2\left(\eta - s(\eta - 1)\right)^2} \right) \right). \tag{6}$$

Here it is also assumed $\gamma = \gamma_0 \eta^{-q}$, where γ_0.= 0.85.[9] The variable q, has not been measured at high pressure, and can have a significant impact on the determined cold curve. We find that a value of q = 0.98 (+0.42, -0.18) yields a cold curve centered on our data (and error bars). This value of q is consistent with static measurements at pressures < 0.1 TPa.[9]

3. Summary of Diamond EOS data

Figure S1 compares our data (initial density $\rho_0 \sim 3.25$ g/cc) with previously reported static,[4] shock Hugoniot,[3-8] and ramp compression[11] data ($\rho_0 \sim 3.515$ g/cc) as stress vs. compression (ρ/ρ_0). Shown as inset to Fig. S1 are calculated stress-compression of the three NIF experiments: N110308, N110516 and N110524 showing the level of repeatability. Figure S2 shows the same curves as S1 albeit in stress-density space. Our ramp-compression data yield slightly lower densities than the calculated isentrope (e.g., ~ 8% offset at 12 g/cm^3) because of initial sample density as well as residual strength/dissipation effects[12]. A simple correction for this low initial density (ρ_0), amounts to scaling the density by the ratio initial densities $(\rho_0^{full} / \rho_0^{sample} = 3.515/3.25)$ so as to compare results at equivalent compression (Fig. S2 black curve) with the DFT cold curve.[13] Figure S3 shows the NIF Data compared to the several Thomas Fermi based isotherms, similar to Fig. 2 in the main paper, only in density space.

1. Aidun J.B. & Gupta Y. M. Analysis of Lagrangian gauge measurements of simple and nonsimple plane waves. *J. Appl. Phys.* **69**, 6998 (1991).
2. Rothman, S. D. *et al.* Measurement of the principle isentropes of lead and lead-antimony alloy to ~400 kbar by quasi-isentropic compression. *J. Phys. D*, **38**, 733-740 (2005).
3. Knudson, M.D., Desjarlais, M.P. & Dolan, D.H. Shock-wave exploration of the high-pressure phases of carbon. *Science* **322**, 1822 (2008).
4. Nagao, H. *et al.* Hugoniot measurement of diamond under laser shock compression up to 2 TPa. *Phys. Plas*. **13**, 052705 (2006).
5. Bradley shock data reported in ref [9].
6. Hicks, D.G. *et al.*, *Phys. Rev. B* **78**, 174102 (2008); Hugoniot data was modified to account for revised Quartz equation-of-state as reported in [Brygoo, S. *et al. Melted quartz as an impedance-match standard for shock studies: further developments.* in preparation (2013).].
7. Brygoo, S. *et al.* Laser-shock compression of diamond and evidence of a negative-slope melting curve. *Nat. Mat.* **6**, 274 (2007).
8. McWilliams, R. S. *et al.*, Strength effects in diamond under shock compression from 0.1 to 1 TPa. *Phys. Rev. B* **81**, 014111 (2010).
9. Dewaele, A., Datchi, F., Loubeyre, P. & Mezouar, M. High pressure-high temperature equation of state of neon and diamond. *Phys. Rev. B* **77**, 094106 (2008).
10. Occelli, F., Loubeyre, P. & Letoullec, R. Properties of diamond under hydrostatic pressures up to 140 GPa. *Nature Mater.* **2**, 151 (2003).
11. Bradley, D.K. *et al.* Diamond at 800 GPa. *Phys. Rev. Letts.* **102**, 075503 (2009).
12. Samples used here have a measured density of 3.25 g/cm^3 : 7.6 % less dense than single crystal diamond. Characterization of our sample material reveals the presence of lower density carbon forms such as graphitic carbon and CH. See the following reference for more details: Dawedeit, C. Grain size dependent physical and chemical properties of thick CVD diamond films for high energy density physics

experiments. *Diamond and related materials*, under review (2013).
13. Martinez-Canales, M., Pickard, C. J. & Needs, R. J. Theormodynamically stable phase of carbon at multiterapascal pressures. *Phys. Rev. Lett.* **108**, 045704 (2012).
14. Lai, D., Abrahams, A. M. & Shapiro, S. L. Equation of state in metals and cold stars: Evaluation of statistical models. *Astrophys. J.* **377**, 612-628 (1991).

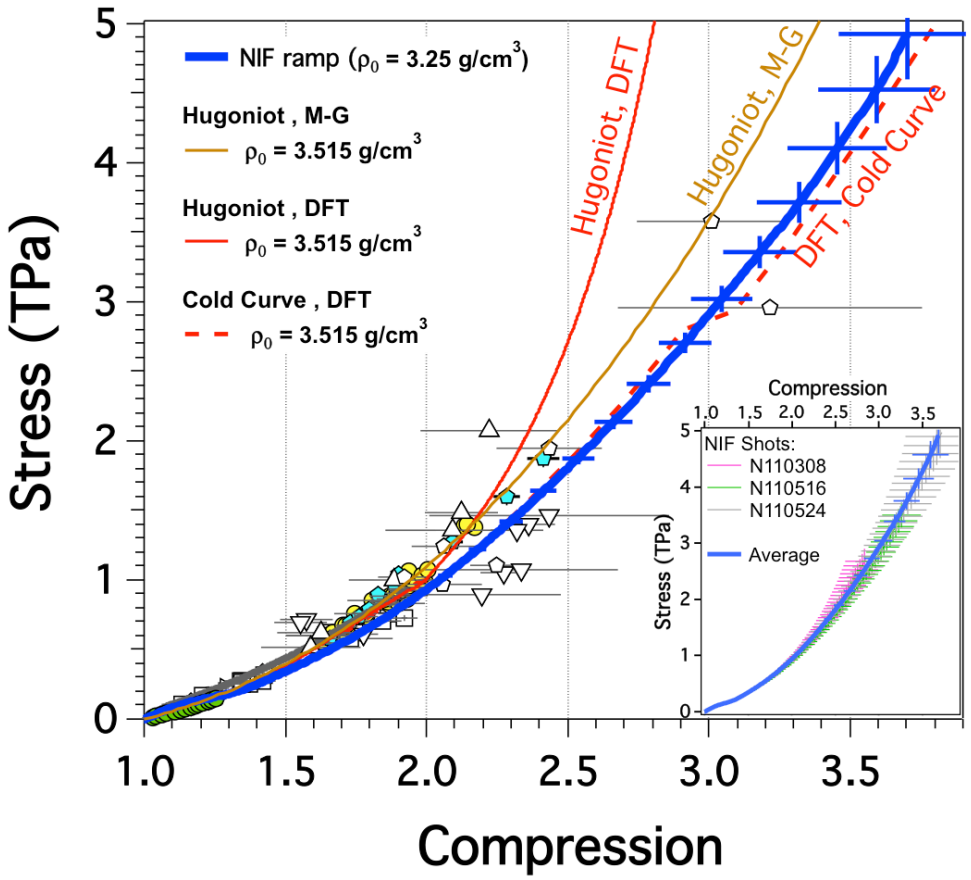

Fig. S1. Stress versus compression for the NIF ramp data (blue solid curve). Also shown are the calculated Hugoniot (solid lines) and the calculated cold curve from DFT (dashed line)[13]. The density shift between the calculated isentrope and cold isotherm are calculated to be negligible. Also shown are data from shock experiments [Knudson[6] (yellow circles), Nagao[7] (up triangle), Bradley[8] (open hexagon), Hicks[9] (blue hexagon), Brygoo[10] (down triangle), MacWilliams[11] (open squares)], isothermal static data [green circles are ruby corrected data from Occelli[4,5]] and the ramp-compression data of Bradley[12] (solid gray curve). Shown as inset are calculated stress-density of the three NIF shots: N110308, N110516 and N110524 showing the level of repeatability between experiments.

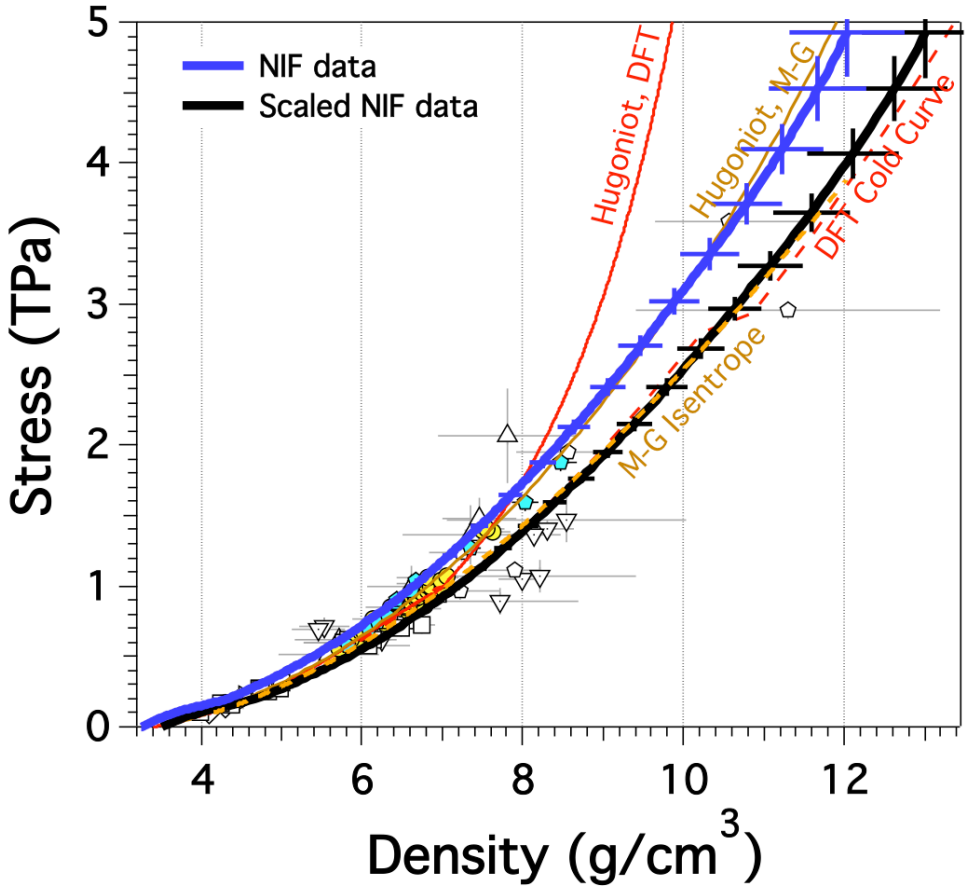

Fig. S2. Stress versus density for the NIF ramp data (blue solid curve). Our ramp-compression data yield slightly lower densities than the calculated isentrope (e.g., ~ 8% offset at 12 g/cm^3) because of the initial density (and possible residual strength) of the sample. A simple correction for this low initial density (ρ_0), amounts to scaling the density by the ratio initial densities ($\rho_0^{full} / \rho_0^{sample} = 3.515/3.25$) so as to compare results at equivalent compression (black curve). Other data and theory are the same as in Fig. S1.

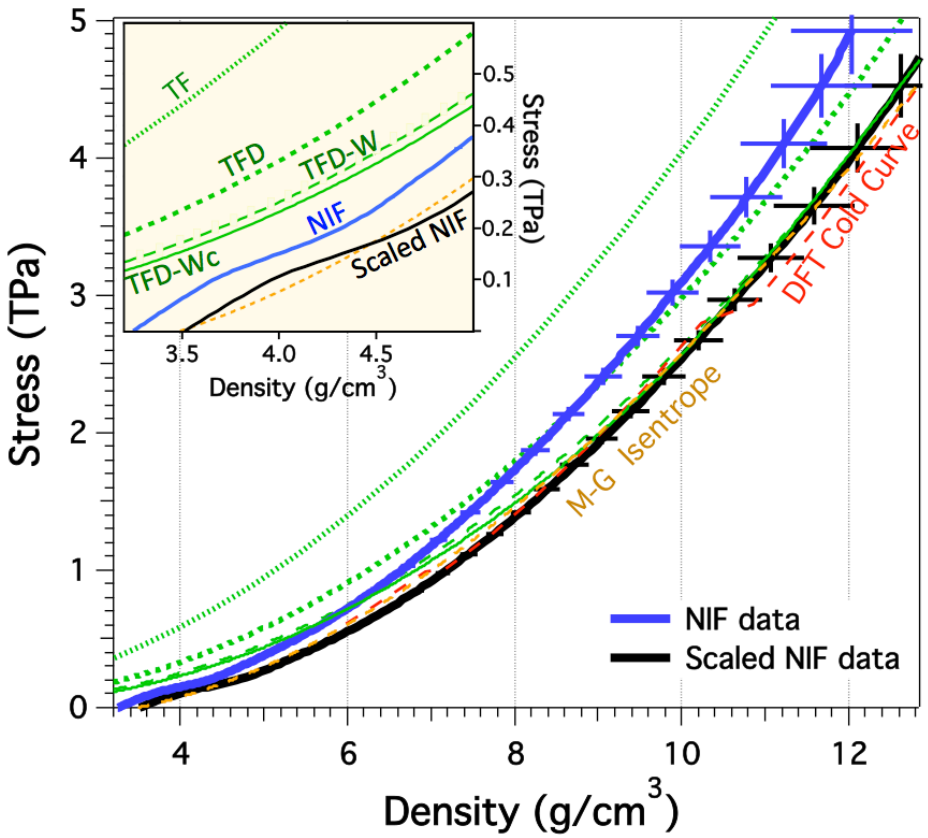

Fig. S3. Stress versus density for the NIF ramp data (blue is raw data and black is the density scaled $(\rho_0^{full} / \rho_0^{sample} = 3.515/3.25)$ data). Model comparisons include: i) the isentrope from DFT (*red dashed curve*), and derived from the extrapolated experimental Hugoniot using a simple Mie-Grueniesen model (*yellow dashed curve*); ii) 0 K isotherms obtained from the statistical-atom models (TF, TFD, TFD-W, and TFD-Wc) as *green dotted, short dashed, long dashed, solid, and dot-dashed curves*)[6]. To present these Thomas-Fermi based isotherms in compression we use the initial density of diamond as the reference density. Central pressures for Earth, Neptune and Saturn are shown for reference[8]. Inset in (*b*) shows detailed comparisons between measurements and models at low pressure.

Table S1.
Calculated Stress-Density Data (blue curve in Figs. 2(b), S1, S2 and S3)

Stress (GPa)	Stress Uncertainty (GPa)	Density (g/cm^3)	Density Uncertainty (g/cm^3)
0.0	0.0	3.25	0.00
9.7	0.1	3.29	0.00
19.5	0.2	3.32	0.00
29.4	0.3	3.36	0.00
39.2	0.3	3.40	0.00
49.2	0.4	3.44	0.00
59.1	0.5	3.48	0.00
69.0	0.6	3.53	0.00
79.0	0.7	3.57	0.00
89.0	0.8	3.61	0.00
98.8	0.8	3.66	0.00
107.8	0.9	3.71	0.00
117.0	1.0	3.76	0.01
125.4	1.1	3.82	0.01
133.8	1.1	3.88	0.01
142.4	1.2	3.94	0.01
151.0	1.3	4.00	0.01
159.7	1.3	4.07	0.01
168.7	1.4	4.13	0.01
178.0	1.5	4.19	0.01
187.8	1.6	4.25	0.01
198.5	1.7	4.31	0.01
210	1.9	4.37	0.01
221	2.0	4.42	0.01
234	2.1	4.48	0.02
247	2.3	4.53	0.02
261	2.4	4.58	0.02
275	2.6	4.63	0.02
289	2.8	4.69	0.02
304	3.0	4.74	0.02
318	3.2	4.79	0.02
333	3.4	4.85	0.02
348	3.6	4.90	0.02

363	3.8	4.95	0.03
379	4.0	5.00	0.03
396	4.3	5.06	0.03
412	4.5	5.11	0.03
428	4.7	5.17	0.03
445	5.0	5.22	0.03
462	5.2	5.27	0.03
480	5.5	5.33	0.04
498	5.8	5.38	0.04
516	6.0	5.44	0.04
534	6.3	5.49	0.04
553	6.6	5.55	0.04
572	6.9	5.60	0.04
592	7.3	5.66	0.05
612	7.6	5.71	0.05
632	7.9	5.77	0.05
653	8.3	5.82	0.05
674	8.7	5.88	0.05
695	9.1	5.93	0.05
717	9.5	5.99	0.06
739	9.9	6.05	0.06
762	10	6.10	0.06
785	11	6.16	0.06
808	11	6.21	0.07
832	12	6.27	0.07
856	12	6.32	0.07
880	13	6.38	0.07
905	13	6.44	0.07
930	14	6.49	0.08
955	14	6.55	0.08
981	15	6.61	0.08
1008	15	6.66	0.09
1035	16	6.72	0.09
1062	17	6.78	0.09
1090	17	6.83	0.09
1118	18	6.89	0.10
1147	19	6.95	0.10
1176	19	7.00	0.10
1205	20	7.06	0.11
1235	21	7.12	0.11
1265	21	7.18	0.11

1296	22	7.23	0.12
1327	23	7.29	0.12
1358	24	7.35	0.12
1390	25	7.41	0.13
1422	25	7.47	0.13
1454	26	7.52	0.13
1487	27	7.58	0.14
1521	28	7.64	0.14
1554	29	7.70	0.14
1588	30	7.76	0.15
1623	31	7.82	0.15
1658	32	7.88	0.16
1694	33	7.94	0.16
1729	34	8.00	0.16
1766	35	8.06	0.17
1802	37	8.12	0.17
1839	38	8.18	0.18
1877	39	8.24	0.18
1915	40	8.31	0.19
1953	42	8.37	0.19
1992	43	8.43	0.20
2032	44	8.49	0.20
2071	46	8.55	0.21
2112	47	8.61	0.21
2152	49	8.68	0.22
2194	50	8.74	0.22
2235	52	8.80	0.23
2277	54	8.86	0.24
2320	55	8.93	0.24
2363	57	8.99	0.25
2406	59	9.05	0.25
2450	60	9.12	0.26
2495	62	9.18	0.27
2540	64	9.25	0.27
2585	66	9.31	0.28
2632	68	9.37	0.28
2678	70	9.44	0.29
2726	72	9.50	0.30
2774	74	9.57	0.30
2822	76	9.63	0.31
2871	79	9.70	0.32

2920	82	9.76	0.33
2969	85	9.83	0.34
3019	88	9.90	0.35
3069	92	9.96	0.36
3119	96	10.03	0.37
3170	100	10.10	0.38
3222	104	10.17	0.39
3273	108	10.23	0.40
3326	112	10.30	0.41
3379	116	10.37	0.42
3432	121	10.44	0.43
3486	125	10.51	0.44
3541	130	10.58	0.45
3596	134	10.65	0.46
3653	139	10.71	0.48
3710	144	10.78	0.49
3768	149	10.85	0.50
3827	155	10.92	0.51
3887	160	10.99	0.53
3947	165	11.06	0.54
4008	171	11.13	0.55
4070	177	11.19	0.56
4133	183	11.26	0.58
4196	189	11.33	0.59
4260	195	11.40	0.61
4324	202	11.47	0.62
4390	208	11.54	0.63
4457	215	11.60	0.65
4524	228	11.67	0.67
4592	242	11.74	0.69
4663	258	11.81	0.72
4736	275	11.87	0.74
4811	293	11.94	0.76
4889	313	12.00	0.79
4929	323	12.03	0.80